CEAS EuroGNC 2019
"Conference on Guidance, Navigation and Control"
3-5 April 2019 @ Politecnico di Milano, Milan, Italy.

CEAS-GNC-2019-030

Minimum drag control allocation for the Innovative Control Effector aircraft

Rob Stolk, and Coen de Visser

Abstract

The Innovative Control Effector model is a tailless delta-wing aircraft concept equipped with 11 control surfaces with overlapping functionality and two-directional thrust vectoring. The high level of redundancy makes it an interesting object for research on mission-specific control allocation. A (spline-based) nonlinear incremental control allocation (INCA) approach is proposed to deal with nonlinear input functions and aerodynamic interaction between multiple control surfaces. The control allocation task is formulated as a weighted least squares problem with variable secondary objectives. Two control allocation modes to minimize drag are proposed and assessed in a general flight scenario. With both modes the average drag is reduced by about 6.5% relative to a standard control allocation scheme. Sensitivity analysis points out that one mode is vulnerable to the choice of initial parameters, whereas the other is primarily sensitive to the accuracy of the onboard model. Improvement of the ICE aerodynamic model is necessary to substantiate the true potential of mission-specific control allocation for next generation aircraft.

1 Introduction

The future air combat environment demands super-maneuverable low-observable fighter aircraft with fault-tolerance capabilities. These features push research toward tailless configurations, as removal of the tail planes increases agility and re-

Rob Stolk
Delft University of Technology, Kluyverweg 1, Delft, The Netherlands e-mail: robstolk92@hotmail.com

Coen de Visser
Delft University of Technology, Kluyverweg 1, Delft, The Netherlands e-mail: c.c.devisser@tudelft.nl

duces the radar cross-section. The loss of control surfaces in the tail area, and the fault-tolerance requirement, necessitates the installation of unconventional control effectors that provide multi-axis moments and redundancy.

An interesting research object in this field is the tailless fighter concept developed under the Innovative Control Effector (ICE) program [1, 2]. The aircraft (Fig. 1) is characterized by its relaxed directional stability, nonlinear dynamics, and a total of 13 effectors with a high level of redundancy and aerodynamic interaction. The large number of effectors and their overlapping functionality however yield challenges in control law design. Since the number of inputs (13 effectors) exceeds the number of directions to control (3 rotations) the control allocation (CA) problem is underdetermined and an infinite number of solutions exists. A convenient way to guide the selection of the 'best' solution is to introduce a secondary objective. Its role is twofold: it provides uniqueness to the solution, while it exploits the excess control power to increase the operational performance of the system. The topic of this paper is to find the lowest aerodynamic drag solution.

Older research proposed generalized-inverse methods for CA such as direct allocation [3], daisy chaining [4], and the redistributed pseudo-inverse [5], because their solutions are feasible with respect to actuator limits and they are computationally cheap. However these methods are proven to produce sub-optimal solutions [6], and, more importantly, they lack the freedom to introduce specified secondary objectives.

More favorable solutions can be generated by constrained quadratic programming (QP) methods. The CA problem is then expressed in a sequential least squares (SLS) or weighted least squares (WLS) form and solved by one of the many available QP solvers. This branch of CA was long considered to be too computationally expensive, but the increase in onboard computational power in the past decade make optimization problems well solvable in real-time nowadays. A more recent development is the incremental nonlinear control allocation (INCA) approach [7] which combines the principles of incremental control [8] with nonlinear dynamic control allocation. INCA naturally includes actuator dynamics and saturation limits and can exploit nonlinear state-actuator and actuator-actuator interactions. In the current paper the mixed objective form is used, minimizing the allocation error and a specific secondary objective in a single step. The solver is based on the active set algorithm from Ref. [9], while the controller architecture is based on the INCA method from Ref. [7].

The main contribution of this paper is the assessment of two CA objectives within the INCA framework to minimize drag for the ICE aircraft. The simplest one only uses a small part of the system model but requires tweaking of certain parameters, while the other is model-based and requires a full internal model of the aerodynamics. The performance of both objectives is analyzed in simulations of a mixed flight mission using two onboard system models with a different degree of accuracy. Because it is considered that future generation fighters feature the same characteristics as the ICE model, the outcome of this research is valuable in control system design for new aircraft with higher performance and lower operational costs.

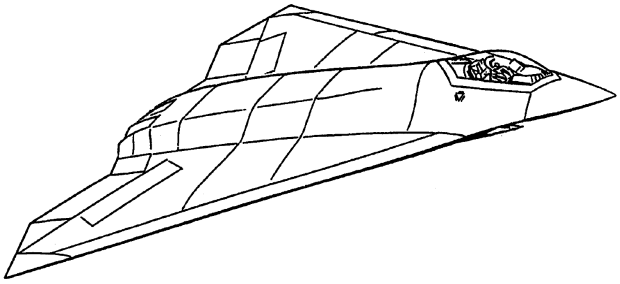

Fig. 1: Sketch of the ICE aircraft [1].

2 Simulation framework

The Innovative Control Effector (ICE) study was a two-phased research started in 1993 [1, 2]. The primary goal was to identify and quantify the aerodynamics and performance of different low-obersevable tailless aircraft configurations with innovative control effectors. This paper focuses on one of the two final designs, the land-based 65 degree leading edge swept delta wing shown in Fig. 1. The model features 13 control effectors: four leading edge flaps (LEFs), two elevons, two all-moving wing tips (AMTs), two spoiler slot deflectors (SSDs), pitch flaps, and thrust vectoring in pitch and yaw direction. An overview of the main modules of the simulation environment is given in Fig. 2. The specifications of the effectors are listed in Table 1.

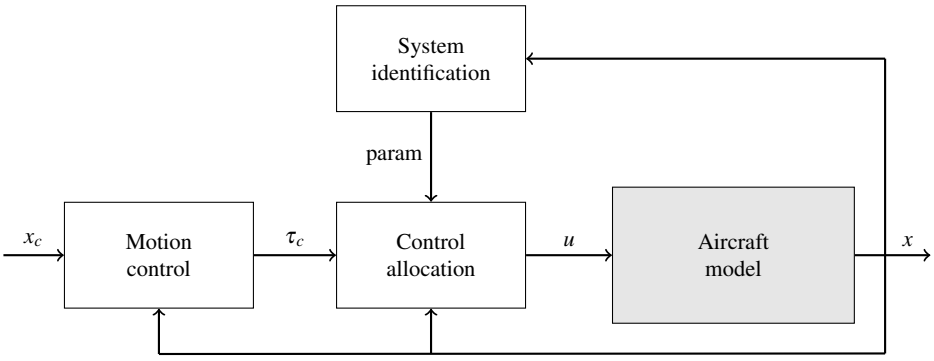

Fig. 2: Block diagram of the simulation setup.

Table 1: Effector specifications.

	Effector	Abbr.	Position limits, deg	Rate limit, deg/s
1	Left inboard leading edge flap (LEF)	llefi	0/40	40
2	Left outboard leading edge flap (LEF)	llefo	-40/40	40
3	Left all-moving wing tip (AMT)	lamt	0/60	150
4	Left elevon	lele	-30/30	150
5	Left spoiler slot deflector (SSD)	lssd	0/60	150
6	Pitch flap	pf	-30/30	150
7	Right inboard leading edge flap (LEF)	rlefi	0/40	40
8	Right outboard leading edge flap (LEF)	rlefo	-40/40	40
9	Right all-moving wing tip (AMT)	ramt	0/60	150
10	Right elevon	rele	-30/30	150
11	Right spoiler slot deflector (SSD)	rssd	0/60	150
12	Pitch thrust vectoring	ptv	-15/15 [a]	150
13	Yaw thrust vectoring	ytv	-15/15 [a]	150

a Thrust vectoring has circular limits. In control allocation pitch and yaw thrust vectoring limits are set to 10.6 deg, such that the combined deflection cannot exceed 15 deg.

II.A Aircraft model

The aerodynamic model consists of 108 data-tables covering wind-tunnel measurements. The six force and moment coefficients C_A, C_Y, C_N, C_l, C_m, C_n are each the sum of 17 to 19 sub-coefficients. These sub-coefficients are a nonlinear function of multiple states and inputs evaluated by linear or cubic interpolation of the wind-tunnel data. Though in some regions the data coverage is sparse, and linear interpolation is doubtful, the model is for now assumed to represent the real behavior of the aircraft. The implementation in MATLAB/Simulink is documented in Ref. [10].

It is noteworthy that the aircraft suffers from severe longitudinal and directional instability under certain circumstances. Furthermore the aerodynamics of the control surfaces are nonlinear and interacting, which means that control effectiveness is affected by the state of the effector, as well as that of other effectors. Examples of the aerodynamics of the model are given in Figs. 3a and 3b.

The aerodynamic model only covers the mainframe and control surfaces aerodynamics. Forces and moments caused by thrust and thrust vectoring are added later on:

$$\begin{aligned} X &= -C_A \cdot {}^1\!/_2 \rho V^2 S + T \cdot \cos(\delta_{ptv}) \cos(\delta_{ytv}) \\ Y &= C_Y \cdot {}^1\!/_2 \rho V^2 S + T \cdot \cos(\delta_{ptv}) \sin(\delta_{ytv}) \\ Z &= -C_N \cdot {}^1\!/_2 \rho V^2 S - T \cdot \sin(\delta_{ptv}) \cos(\delta_{ytv}) \\ l &= C_l \cdot {}^1\!/_2 \rho V^2 S b \\ m &= C_m \cdot {}^1\!/_2 \rho V^2 S \bar{c} - T \cdot l_{tv} \sin(\delta_{ptv}) \cos(\delta_{ytv}) \\ n &= C_n \cdot {}^1\!/_2 \rho V^2 S b - T \cdot l_{tv} \cos(\delta_{ptv}) \sin(\delta_{ytv}) \end{aligned} \tag{1}$$

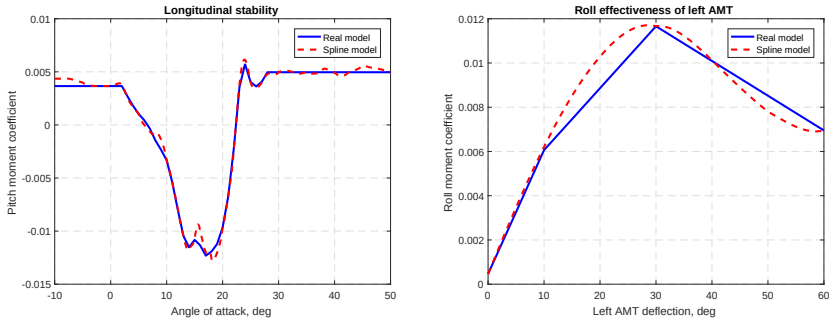

(a) (b)

Fig. 3: Insight in the ICE aerodynamics at Mach 0.6.

X,Y,Z are the boxy forces and l,m,n the body moments in a right-handed axis system with X pointing forward and Z pointing downward. ρ is the air density, V the total airspeed, S the wing surface, and b and $\bar{c}$ the wing span and mean aerodynamic chord. T is the thrust force and l_{tv} the arm of thrust vectoring.

The original implementation discussed in Ref. [10] does not include actuator dynamics and limits. These are added between the controller and the aircraft model using transfer functions, rate limits and position limits in that order. Position and rate limits are given in Table 1. For the leading edge flaps the dynamics are represented by

$$\frac{\delta}{\delta_c}(s) = 18 \cdot \frac{400}{(s+18)(s+100)} \tag{2}$$

and for all other effectors by

$$\frac{\delta}{\delta_c}(s) = 40 \cdot \frac{400}{(s+40)(s+100)} \tag{3}$$

with δ the real deflection and δ_c the commanded deflection. Because the gain of both transfer functions is 4, actuator control consists of a gain of 1/4. No more detailed actuator controller is applied for now.

II.B Nonlinear Dynamic Inversion

This section briefly describes the control laws implemented in the motion control module from Fig. 2. Consider the equations of motion in the affine form:

$$\dot{x} = f(x) + g(x)\tau \tag{4}$$

$$\tau = \Phi(x,u) \tag{5}$$

in which $x \in \mathbb{R}^n$ is the state vector, $\tau \in \mathbb{R}^l$ is the vector of moment coefficients, and $u \in \mathbb{R}^m$ is the input vector. Control of these systems is commonly separated in two parts: motion control to calculate the required moment (τ_c) to track a reference signal, and control allocation to spread the required moment over the available effectors.

The motion controller in this research is based on the nonlinear dynamic inversion (NDI) theory. The control laws are derived in Ref. [11]. For the control of the body angular rates Eq. 4 reads as follows:

$$\begin{bmatrix} \dot{p} \\ \dot{q} \\ \dot{r} \end{bmatrix} = -I^{-1} \left(\begin{bmatrix} p \\ q \\ r \end{bmatrix} \times I \begin{bmatrix} p \\ q \\ r \end{bmatrix} \right) + \frac{1}{2} \rho V^2 S I^{-1} \begin{bmatrix} b & 0 & 0 \\ 0 & \bar{c} & 0 \\ 0 & 0 & b \end{bmatrix} \begin{bmatrix} C_l \\ C_m \\ C_n \end{bmatrix} \tag{6}$$

in which I is the moment of inertia. Inversion of this system results in the following function for the moment command τ_c:

$$\begin{bmatrix} C_l \\ C_m \\ C_n \end{bmatrix}_c = \frac{I}{\frac{1}{2}\rho V^2 S} \begin{bmatrix} b & 0 & 0 \\ 0 & \bar{c} & 0 \\ 0 & 0 & b \end{bmatrix}^{-1} \left\{ \begin{bmatrix} \dot{p} \\ \dot{q} \\ \dot{r} \end{bmatrix}_c + I^{-1} \left(\begin{bmatrix} p \\ q \\ r \end{bmatrix} \times I \begin{bmatrix} p \\ q \\ r \end{bmatrix} \right) \right\} \tag{7}$$

in which $\begin{bmatrix} \dot{p} & \dot{q} & \dot{r} \end{bmatrix}_c^T$ is the commanded angular acceleration set by a linear outer loop controller. Additionally an aerodynamic NDI outer loop is implemented to control the angle of attack α, angle of sideslip β and roll angle ϕ. The control laws are derived in Ref. [11].

II.C System identification

Model-based control requires an estimation of the system parameters. As will be made clear in the remainder of this paper, for control allocation the current forces and moments acting on the aircraft, and their derivatives to every input are essential information. A system identification module is implemented in the simulation framework, based on the following.

Exact model

An exact estimation of the system parameters can be obtained by copying the 'real' table-based aerodynamic model from section II.A into the system identification module. Feeding in the current states (x_0) and inputs (u_0) gives the current force- and moment coefficients C_{X_0}, C_{Y_0}, C_{Z_0}, C_{l_0}, C_{m_0}, and C_{n_0}. Because the functions are not analytic, derivatives with respect to the inputs cannot mathematically be derived. They can however be obtained by the taking the central difference of the parameter values with one input slightly increased and decreased. For this study the central dif-

ference approximation with $u_i^+ = u_{i,0} + 0.1$ deg and $u_i^- = u_{i,0} - 0.1$ deg is applied, such that

$$\frac{\partial C}{\partial u_i} = \frac{C(x_0, u_0, u_i^+) - C(x_0, u_0, u_i^-)}{u_i^+ - u_i^-} \tag{8}$$

Because thrust vectoring is not a part of the aerodynamic model, its contribution to the force- and moment coefficients and their derivatives are established according to the equations in Table 2.

Table 2: Thrust vectoring model in system identification.

C	$\frac{\partial C}{\partial \delta_{ptv}}$	$\frac{\partial C}{\partial \delta_{ytv}}$
C_X $+\frac{T}{1/2\rho V^2 S}\cos(\delta_{ptv})\cos(\delta_{ytv})$	$-\frac{T}{1/2\rho V^2 S}\sin(\delta_{ptv})\cos(\delta_{ytv})$	$-\frac{T}{1/2\rho V^2 S}\cos(\delta_{ptv})\sin(\delta_{ytv})$
C_Y $+\frac{T}{1/2\rho V^2 S}\cos(\delta_{ptv})\sin(\delta_{ytv})$	$-\frac{T}{1/2\rho V^2 S}\sin(\delta_{ptv})\sin(\delta_{ytv})$	$\frac{T}{1/2\rho V^2 S}\cos(\delta_{ptv})\cos(\delta_{ytv})$
C_Z $-\frac{T}{1/2\rho V^2 S}\sin(\delta_{ptv})\cos(\delta_{ytv})$	$\frac{T}{1/2\rho V^2 S}\cos(\delta_{ptv})\cos(\delta_{ytv})$	$\frac{T}{1/2\rho V^2 S}\sin(\delta_{ptv})\sin(\delta_{ytv})$
C_m $-\frac{Tl_{tv}}{1/2\rho V^2 S\bar{c}}\sin(\delta_{ptv})\cos(\delta_{ytv})$	$-\frac{Tl_{tv}}{1/2\rho V^2 S\bar{c}}\cos(\delta_{ptv})\cos(\delta_{ytv})$	$\frac{Tl_{tv}}{1/2\rho V^2 S\bar{c}}\sin(\delta_{ptv})\sin(\delta_{ytv})$
C_n $-\frac{Tl_{tv}}{1/2\rho V^2 Sb}\cos(\delta_{ptv})\sin(\delta_{ytv})$	$\frac{Tl_{tv}}{1/2\rho V^2 Sb}\sin(\delta_{ptv})\sin(\delta_{ytv})$	$-\frac{Tl_{tv}}{1/2\rho V^2 Sb}\cos(\delta_{ptv})\cos(\delta_{ytv})$

Spline model

The central difference method to calculate force- and moment derivatives requires 22 extra evaluations of the six main coefficients, namely twice for every control surface. With an analytic model of the aircraft, the control derivatives can be calculated mathematically at a lower computational cost. In Ref. [12] a multivariate simplex B-spline model of the ICE aerodynamics is developed. Splines are piecewise polynomial approximations of a function defined in barycentric coordinates. They are known for their flexibility and remarkable competence to model nonlinear systems with local irregularities. The spline model of the ICE aircraft from Ref. [12] has an accuracy unable to achieve with an ordinary polynomial model, though it is not perfect as can be seen in Fig. 3. The use of this model for system identification reveals the sensitivity of the to be developed controller to model inaccuracies. Calculating the derivatives of the force- and moment functions (in barycentric space) with respect to physical inputs (in Cartesian space) is already researched and documented in Ref. [11]. Note that the spline model only covers the aerodynamics, so it is also expanded with the thrust vectoring model from Table 2.

3 Incremental control allocation

The motion controller from section II.B sets the commanded moment coefficients τ_c such that the reference signal x_c is tracked. It is the task of control allocation

(CA) to spread this control demand over the available inputs u. Most existing CA methods consider a linear effector model, such that Eq. 5 can be written in the affine form

$$\tau = B(x)u \tag{9}$$

with B called the control effectiveness matrix. The linear system from Eq. 9 is efficient for solvers, but it is also limited in three ways. At first it assumes that τ is caused purely by inputs, leaving the aircraft mainframe aerodynamics out of the equation. Secondly it assumes that the control effectiveness is constant over the entire range of the effector. Finally it does not account for aerodynamic interactions between effectors. All three assumptions are not valid for the ICE aircraft.

A more accurate approach is to locally linearize the system about the current state and inputs, as is described in Ref. [13] and for the spline-based variant in Ref. [11]. The idea is then that input increments are calculated based on the control demand increment [7]. Consider the form

$$\begin{aligned} \tau &= \tau_0(x,u_0) + B(x,u_0)\Delta u \\ u &= u_0 + \Delta u \end{aligned} \tag{10}$$

such that τ_0 represents the current moment vector and B is the incremental control effectiveness matrix containing local control derivatives. In fact B is the Jacobian of the control directions w.r.t the inputs, evaluated at the current state and inputs:

$$B(x,u_0) = \begin{bmatrix} \left.\frac{\partial C_l}{\partial u_1}\right|_{x,u_0} & \cdots & \left.\frac{\partial C_l}{\partial u_m}\right|_{x,u_0} \\ \left.\frac{\partial C_m}{\partial u_1}\right|_{x,u_0} & \cdots & \left.\frac{\partial C_m}{\partial u_m}\right|_{x,u_0} \\ \left.\frac{\partial C_n}{\partial u_1}\right|_{x,u_0} & \cdots & \left.\frac{\partial C_n}{\partial u_m}\right|_{x,u_0} \end{bmatrix} \tag{11}$$

See Fig. 4 for a graphic explanation of the difference between global and local control effectiveness estimation. As long as input increments are small, so the update frequency of the controller is high, INCA is a powerful tool to deal with nonlinear and coupled input dynamics.

One important feature of the ICE model not taken into account for now are non-monotonic nonlinearities in the input dynamics. Parabolic functions such as in Fig. 3b can be misleading if control effectiveness is evaluated beyond the slope reversal. Although for now this phenomenon is not encountered in practice, it is worthwhile a more detailed analysis in future research.

Incremental control allocation can be applied to both generalized inverse methods and optimization-based CA. The unconstrained pseudo-inverse [14] for example can just as well be used to calculate the input increment:

$$\begin{aligned} \Delta u &= B^{+}(\tau_c - \tau_0) + (I - B^{+}B)(u_p - u_0) \\ u &= u_0 + \Delta u \end{aligned} \tag{12}$$

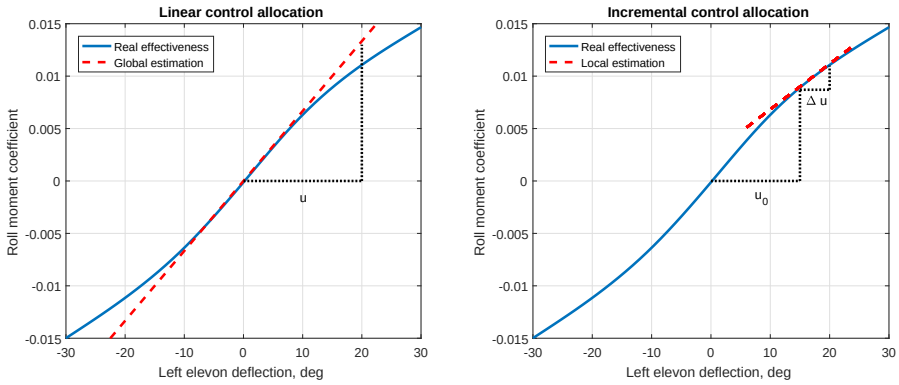

Fig. 4: Explanation of linear CA and INCA. Local linearization about u_0 and calculating the increment Δu gives a better estimation of the real control effectiveness at $u = u_0 + \Delta u$.

but keep in mind to subtract u_0 from the preferred input. For the ICE model however a weighted least squares (WLS) optimization is suggested. If the secondary objective is to force the inputs to a preferred state (u_p), the CA problem becomes

$$\min_{\Delta u} \|Q(B\Delta u + \tau_0 - \tau_c)\|_2 + \left\|W(\Delta u + u_0 - u_p)\right\|_2 \tag{13}$$
$$\text{subj. to } \underline{u} \leq \Delta u \leq \overline{u}$$

with

$$\begin{aligned} \underline{u} &= \max(-\dot{u}, u_{\min} - u_0) \\ \overline{u} &= \min(\dot{u}, u_{\max} - u_0) \end{aligned} \tag{14}$$

Q and W are weighting matrices to prioritize allocation in certain directions or minimizing certain inputs. $Q \gg W$ should be used to emphasize the importance of allocation error minimization over control minimization. $\|\cdot\|_2$ represents the l_2-norm and is defined as

$$\|a\|_2 = \left(\sum_{i=1}^{\dim(a)} |a_i|^2 \right)^{(1/2)} \quad \text{(Ref. [13])} \tag{15}$$

Equation 13 can be solved by one the of the many available quadratic programming methods. In this research active set programming is used, based on Ref. [13], solving the primary and secondary objective in one step, e.g.

$$\min_{\underline{u} \leq \Delta u \leq \overline{u}} \left\| \begin{pmatrix} QB \\ W \end{pmatrix} \Delta u + \begin{pmatrix} Q(\tau_0 - \tau_c) \\ W(u_0 - u_p) \end{pmatrix} \right\|_2 \tag{16}$$

4 Minimum drag objective

Previous research focused on optimization-based CA algorithms to solve Eq. 13 with fixed secondary objectives. The most common choice is

$$W = \text{diag}(1,1,1,1,1,1,1,1,1,1,1,1,1) \qquad (17)$$
$$u_p = \left[0,0,0,0,0,0,0,0,0,0,0,0,0\right]^T$$

which minimizes the total control effort. In general this strategy comes up with a convenient set of inputs, but the focus here is on the uniqueness of the solution rather than on its physical impact.

Given the excessive number and diverse nature of the controls on the ICE aicraft, it is considered that more though-out secondary objectives can yield a significant improvement of the operational performance. This section proposes two control allocation strategies to reduce the aerodynamic drag of the aircraft.

IV.A Effector prioritization

James M. Buffington [15] first experimented with exploiting the redundancy of the ICE aircraft using mission-specific W-matrices. The idea is that a higher W-value penalizes the deflection of an effector, such that the use of the others is prioritized. To minimize the wing loading the AMTs were penalized, whereas for the minimum radar cross-section mode the SSDs were given the highest W-value.

The same can be applied to decrease aerodynamic drag. The weighing matrix has to penalize the most resistant controls, such that their use is avoided if the control power is sufficient. It is found that for the ICE aircraft the SSDs generally cause the most drag and the leading edge flaps and thrust vectoring the least. Hence the following weighing is chosen:

$$W = \text{diag}(1,1,5,5,10,5,1,1,5,5,10,1,1) \qquad (18)$$
$$u_p = \left[0,0,0,0,0,0,0,0,0,0,0,0,0\right]^T$$

Note that the order of the effectors is given in Table 1.

Although the values in Eq. 18 are based upon an analysis of the system and iterative experiments, they might not be the most suitable in every single situation. This is inherent to fixed-value control allocation objectives.

IV.B Model-based

It is also possible to deviate from the regular secondary objective formulation with W and u_p, and in fact introduce an analytic expression for drag. The optimization objective becomes

$$\min_{\underline{u}\leq\Delta u\leq\overline{u}} \|Q(B\Delta u+\tau_0-\tau_c)\|_2+\|(C_D(x,u))\|_2 \tag{19}$$

In order for the minimum drag objective to fit in the WLS incremental form, drag first has to be expressed as an affine function of Δu. That is achieved as follows. The drag coefficient is defined as the negative force coefficient in X-direction in the aerodynamic frame. The force coefficients in the aerodynamic frame are calculated by the following transformation:

$$\begin{bmatrix} C_X' \\ C_Y' \\ C_Z' \end{bmatrix} = \begin{bmatrix} \cos\alpha & 0 & \sin\alpha \\ 0 & 1 & 0 \\ -\sin\alpha & 0 & \cos\alpha \end{bmatrix} \begin{bmatrix} \cos\beta & \sin\beta & 0 \\ -\sin\beta & \cos\beta & 0 \\ 0 & 0 & 1 \end{bmatrix} \left(\begin{bmatrix} C_X \\ C_Y \\ C_Z \end{bmatrix} - \begin{bmatrix} C_T \\ 0 \\ 0 \end{bmatrix} \right) \tag{20}$$

in which $C_T = \frac{T}{{}^1\!/_2\rho V^2 S}$ is the thrust coefficient. This term has to be subtracted to make sure drag only consists of control surface resistance and the loss of thrust in forward direction due to thrust vectoring. This loss is considered to be $T\cdot(1-\cos\delta_{ptv}\delta_{ytv})$. Given Eq. 20

$$C_D = -C_X' = -C_X\cos(\alpha)\cos(\beta) - C_Y\cos(\alpha)\sin(\beta) - C_Z\sin(\alpha) + C_T\cos(\alpha)\cos(\beta) \tag{21}$$

with $C_X(x,u)$, $C_Y(x,u)$, and $C_Z(x,u)$ in the body frame as recorded in the model. The drag coefficient is a linear combination of the force coefficients in the body frame, so the drag derivative w.r.t. an input is

$$\frac{\partial C_D}{\partial u_i} = -\frac{\partial C_X}{\partial u_i}\cos(\alpha)\cos(\beta) - \frac{\partial C_Y}{\partial u_i}\cos(\alpha)\sin(\beta) - \frac{\partial C_Z}{\partial u_i}\sin(\alpha) \tag{22}$$

The derivatives toward all inputs are combined in the drag effectiveness matrix

$$E(x,u_0) = \begin{bmatrix} \frac{\partial C_D}{\partial u_1}\Big|_{x,u_0} & \cdots & \frac{\partial C_D}{\partial u_m}\Big|_{x,u_0} \end{bmatrix} \tag{23}$$

and so the incremental drag formula reads

$$C_D = C_{D_0}(x,u_0) + E(x,u_0)\Delta u \tag{24}$$

The model-based minimum drag CA problem is then as follows:

$$\min_{\underline{u}\leq\Delta u\leq\overline{u}} \|Q(B\Delta u+\tau_0-\tau_c)\|_2+\left\|E\Delta u+C_{D_0}\right\|_2 \tag{25}$$

The secondary objective in Eq. 25 does not 'know' the exact minimum drag position of the effectors. Rather the incremental nature implies a gradient decent search toward this position. The magnitude of each E-value represents the amount of resistance per unit increment of the particular effector, while the sign of the E-value indicates if the minimum drag position is higher or lower than the current position. If Q is chosen too low, drag is considered more important than the allocation error, and the effectors are indeed driven toward their minimum drag position in a couple of time steps, but the aircraft destabilizes. Appropriate Q-values are found to be in the range of 5 to 10.

At first instance the method described looks to be related to a control minimization objective (Eq. 13) with $W = \text{diag}|E|$ and u_p the minimum drag position. Though W is in that scenario treated as the global drag effectiveness from u_p to u_0, while $|E|$ actually represents the local resistance about u_0. Moreover finding the minimum drag position each time step for each effector requires a lot of computations, making the approach from Eq. 25 far more useful.

Please also note that the objective from Eq. 25 has only 3 parameters (3 Q-values), whereas Eq. 13 has 29 (3 Q-values, 13 W-values, and 13 u_p-values). Hence the model-based objective requires a lot less tuning, for it gets most information through system identification. This makes the method less sensitive to preliminary decisions, but more to modeling errors.

5 Results

Three control allocation modes with different secondary objectives are evaluated in a mixed flight scenario. All modes are in incremental form and solved by the active set algorithm from section 3. The names, abbreviations, optimization objectives, and other settings are as follows.

- Standard mode (ST)

$$\min_{\underline{u}\leq\Delta u\leq\overline{u}} \left\| \begin{pmatrix} QB \\ W \end{pmatrix} \Delta u + \begin{pmatrix} Q(\tau_0 - \tau_c) \\ W u_0 \end{pmatrix} \right\|_2 \tag{26}$$

$$Q = \text{diag}(10000, 10000, 10000)$$
$$W = \text{diag}(1,1,1,1,1,1,1,1,1,1,1,1,1)$$

- Prioritization mode (PR)

$$\min_{\underline{u}\leq\Delta u\leq\overline{u}} \left\| \begin{pmatrix} QB \\ W \end{pmatrix} \Delta u + \begin{pmatrix} Q(\tau_0 - \tau_c) \\ Wu_0 \end{pmatrix} \right\|_2 \tag{27}$$

$$Q = \text{diag}(20000, 20000, 20000)$$
$$W = \text{diag}(1,1,5,5,10,5,1,1,5,5,10,1,1)$$

- Model-based mode (MB)

$$\min_{\underline{u}\leq\Delta u\leq\overline{u}} \left\| \begin{pmatrix} QB \\ E \end{pmatrix} \Delta u + \begin{pmatrix} Q(\tau_0 - \tau_c) \\ C_{D_0} \end{pmatrix} \right\|_2 \tag{28}$$

$$Q = \text{diag}(5,5,5)$$

The Q-matrices are chosen such that the relative importance of all secondary objectives is about equal.

V.A Flight with exact model

The flight test consists of moderate maneuvering with roll and sideslip (aiming) commands at Mach 0.6 at 600 ft altitude. After 5 seconds of stabilization a 5 second left turn is taken in a bank angle of -30 degrees. Between 15 and 20 seconds a -20 degrees angle of sideslip command is given. The mission ends with a steep right turn of half a minute in a bank angle of 60 degrees. It is known that especially the latter maneuver is important in air combat, but often limited by the available power. Drag reduction in this scenario increases the odds over the competitor.

For assessment altitude is kept constant through an outer loop controlling the angle of attack. Constant thrust is set to 6500 lbf. No climbing maneuvers are included in the simulation, because it is found in a climb situation most drag, both from the mainframe and from the effectors, is lift-induced drag. For a given angle of attack it is possible to reduce drag by placing control surfaces parallel to the airflow, but this will be accompanied by a decrease of lift. To compensate for that, a higher angle of attack has to be flown and the drag reduction in the end is not significant.

The attitude response, airspeed, altitude, and aerodynamic drag are shown in Fig. 5. The values of average drag are given in Table 3. For clarity of the graphs the turbulence model is turned off, but drag values of simulations with turbulence are also given in Table 3.

It is clear from Fig. 5 that under constant bank angles ($5s-10s$ and $25s-55s$) the PR-mode and MB-mode reduce drag with respect to the ST-mode. Also sideslip commands ($15s-20s$) are well tracked by these modes, while reducing drag with about 8% relative to the standard mode. The difference in average drag values between the PR-mode and MB-mode is from Table 3 not significant, but from Fig. 5d it may be clear that the PR-mode is beneficial during the dynamic part of the

Table 3: Results of flight with exact model.
ST = standard mode, PR = prioritization mode, MB = model-based mode.

Mode	Average drag [lbf]	
	turbulence off	*turbulence on*
ST	6462.6	6503.1
PR	6041.2 (−6.52%)	6098.6 (−6.22%)
MB	6046.1 (−6.44%)	6080.1 (−6.51%)

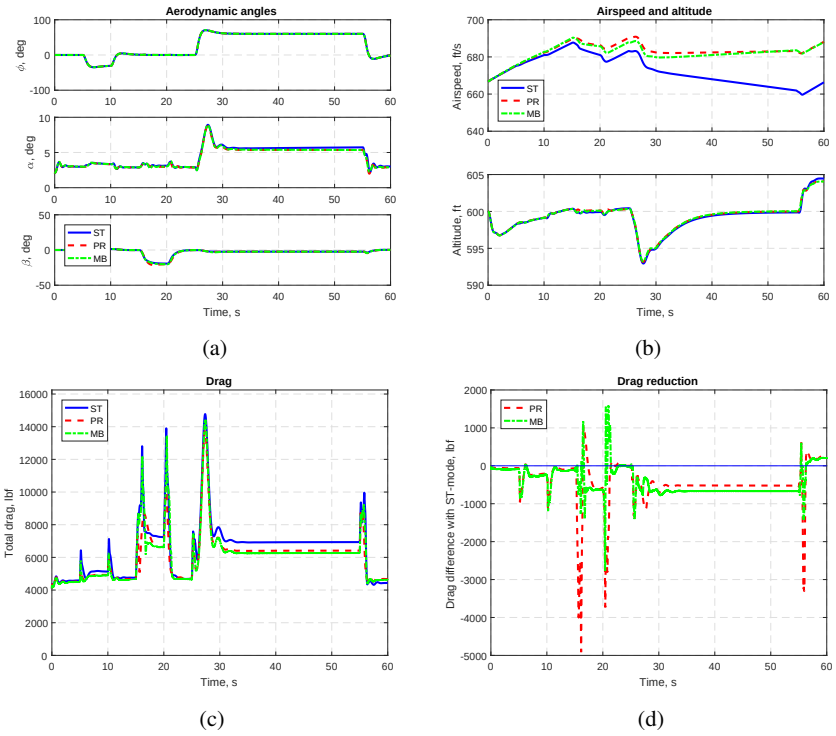

Fig. 5: Aerodynamic angles, airspeed, altitude, and drag during flight with exact model.
ST = standard mode, PR = prioritization mode, MB = model-based mode.

maneuver, whereas the MB-mode reduces more drag in the steady parts. Overall the PR-mode performs slightly better, though in turbulence it is the other way around. Notice that in cruise flight drag reduction is not significant, which is the reason that climb maneuvers are not investigated for now.

It is interesting to look how the minimum drag modes accomplish the drag reduction. Figs. 6a and 6b show the effector positions in the steady part of the sideslip maneuver (at 19s) and right turn (at 35s) respectively. Some specific choices are clear. Whereas the ST-mode uses primarily the left SSD in a sideslip, the PR-mode

selects yaw thrust vectoring and the left outboard LEF, and the MB-mode chooses yaw thrust vectoring and the right inboard LEF. To suppress sideslip in the right turn the ST-mode again uses the yaw power of the left SSD, and the other modes choose thrust vectoring.

It looks like the most drag reduction can be achieved by just keeping the SSDs closed. A simulation with only this constraint already shows a drag reduction of almost 5%. At low angles of attack the SSDs are indeed a poor choice for yaw control because they generate a lot of drag and degrade the effectiveness of the elevons. Though in extreme situations extra yaw power can be necessary, and additionally the SSDs are very useful at high angles of attack to recover airflow over the trailing edge flaps.

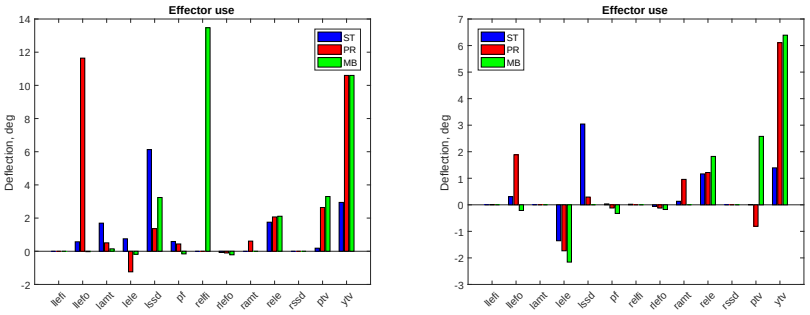

(a) Effector states during sideslip, measured at 19s.

(b) Effector states during sideslip, measured at 35s.

Fig. 6: Effector use during steady parts of the mission.
ST = standard mode, PR = prioritization mode, MB = model-based mode.

V.B Flight with spline model

In the previous simulations the onboard model of the system is assumed perfect, i.e. τ_0, B, C_{D_0}, and E used in control allocation are the exact values. This however is an utopia, since the internal model always has some degree of inaccuracy. The same mission if therefore flown with the spline model from section II.C delivering information to the control allocation module. The aerodynamic angles, airspeed, altitude, and drag plots are given in Fig. 7.

From Figs. 7a and 7b it can be concluded that the tracking performance is similar to when an exact model is used (Figs. 5a and 5b). Hence the spline model is accurate enough for decent operation, at least for the kinds of maneuvers tested. Also the drag values of the ST-mode and PR-mode are comparable.

Table 4: Results of flight with spline model.
ST = standard mode, PR = prioritization mode, MB = model-based mode.

Mode	Average drag [lbf]	
	turbulence off	*turbulence on*
ST	6523.2	6588.8
PR	6174.4 (−5.35%)	6218.8 (−5.62%)
MB	6307.6 (−3.30%)	6362.4 (−3.44%)

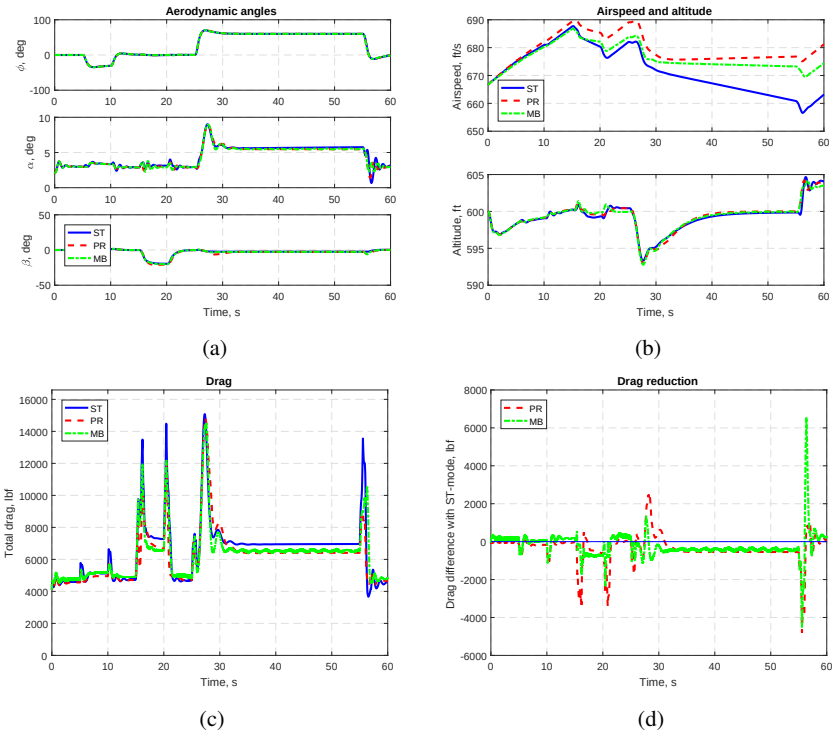

Fig. 7: Aerodynamic angles, airspeed, altitude, and drag during flight with spline model.
ST = standard mode, PR = prioritization mode, MB = model-based mode.

However from Table 4 and Fig. 7d it can be deduced that the performance of the MB-mode is notably degraded by the use of the spline model. The reason for this is that an imperfect model sometimes provides misleading (drag-)information to the controller. See for example Fig. 8. According to the spline model the deflection of the left AMT can be a couple of degrees without producing much drag. In reality however the drag is significantly higher, up to 8% at $\delta_{lamt} = 4$ deg. The aerodynamic model consists of 108 sub-models, each of them with this kind of inaccuracies, adding up to the loss in performance of the MB-mode. The PR-mode does not use

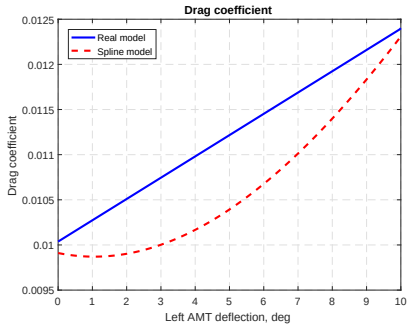

Fig. 8: Drag coefficient vs. left AMT deflection at Mach 0.6 and $\alpha = 3$ deg.

this information, so its drag reduction capability is less affected by the quality of the model.

V.C Discussion

From Tables 3 and 4 it can be concluded that mission specific control allocation can indeed optimize operational performance, in this case drag reduction. The advantages are most apparent in the steady states of a turn or aiming maneuver, and in the roll-in and roll-out phase. In cruise flight the drag reduction is marginal. The validity of the comparison of drag values is proven by Figs. 5 and 7. Under all three modes the same maneuver is flown: altitude is kept constant and the aerodynamic angle tracking exactly matches. Each test the thrust setting is the same, but the final airspeeds of the PR-mode and MB-mode are higher than that of the ST-mode. This indicates that the aircraft encountered less resistance along the way. When thrust for the PR-mode and MB-mode is set to 6100 lbf the final airspeeds are comparable (with the exact model), underlining these modes make the aircraft more full efficient.

The simulations described are performed at Mach 0.6 at an altitude of 600 ft. Simulations of the same maneuvers in other conditions prove that the performance is maintained, see e.g. Figs. 9a. The PR-mode turns out to be more sensitive to Mach number than the MB-mode. The influence of altitude is negligible for both modes. The maneuvers are not very suitable for supersonic flight or high altitudes, so the ability of drag reduction in this part of the flight envelope is a topic for future research. Fig. 9b shows the drag reduction in a right turn with various bank angles. The sharper the turn, the more drag is reduced. It is also clear that the MB-mode outperforms the PR-mode, primarily in the steady part as is argued earlier. Steeper bank angles than 60 degrees can be flown, but the aircraft easily destabilizes. Better tuning of the outer loops and flight envelope protection is required for further testing.

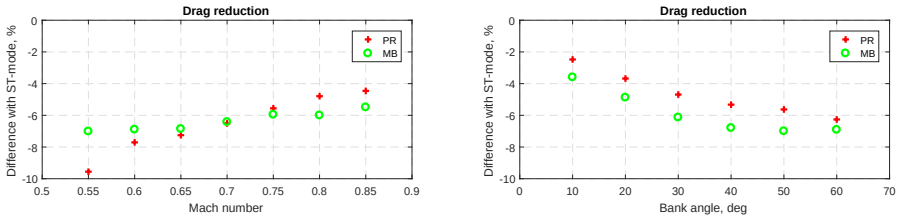

(a) Drag reduction at various Mach numbers. Maneuver is the same as previously. Altitude is 10000 ft.

(b) Drag reduction at various bank angles. Maneuver consists of 5 seconds cruise, 20 seconds turn, and 5 seconds cruise. Mach 0.6 at 600 ft.

Fig. 9: Drag reduction at various Mach numbers and at various bank angles with exact model.
ST = standard mode, PR = prioritization mode, MB = model-based mode.

All in all, both minimum drag modes are able to reduce the operation drag of the ICE aircraft, and it turns out that the PR-mode produces better solutions if the on-board model lacks accuracy, as was expected. But does this make the PR-mode the preferred technique in practical applications? As mentioned earlier the MB-mode has a lot less parameters to be manually tuned than the PR-mode. Moreover the performance of the MB-mode turns out to be rather robust to the choice of Q-values, as long as the importance of the primary objective is clear ($Q \geq 5$). The reason for this is that in most situations, especially in the steady parts of the mission, the allocation error can easily be minimized to zero, so the relative importance of the secondary objective does not play a role. Practically speaking control allocation does not have to make a concession between primary and secondary objective, because the primary objective can be achieved to the fullest, leaving enough excess power for the secondary objective whatever Q-value.

On the other hand, the PR-mode *is* very sensitive to the choice of its parameters. In fact the entire power of PR-mode relies on the iterative establishment of W-values. For example a simulation with a slightly different $W = \text{diag}(1,1,5,5,5,5,1,1,5,5,5,2,2)$, shows that the drag reduction capability is more than halved: -3.10% against -6.52% originally. The W-matrix in this study is specifically optimized for the maneuvers performed, but in an other mission it can behave differently. This vulnerability of the PR-mode is inherent to its design and makes the MB-mode a preferable option in systems of which the dynamics are accurately mapped.

A final point of attention is that the model now assumed to be 'real' is in some parts very illogical. Linear interpolation of sparse data results in implausible input dynamics, see e.g. Fig. 3b. Multivariate simplex splines are not able to capture such sharp functions, which explains most of the inaccuracy of the spline model. In reality though, the aircraft is expected to feature smoother input dynamics, and the spline model will not be that imprecise. The drop is performance of the MB-mode by the use of the spline model is thus exaggerated in this study.

6 Conclusions

The next generation fighter aircraft is likely to feature a tailless design with control surfaces for pitch and yaw relocated on the main wing. The large number of effectors and their overlapping functionality requires a smart control allocation approach that comes up with a unique and operationally attractive solution. This research focused on decreasing drag of the ICE aircraft through two specifically designed secondary control allocation objectives.

The first drag minimization mode (prioritization, PR) penalizes the deflection of the most drag-causing effectors, such that the use of low-resistant effectors is preferred. In the mission flown, the PR-mode reduces drag with about 6% relative to the standard control allocation mode. The reduction is primary the result of using thrust vectoring instead of the SSDs for yaw control. The performance of the PR-mode is relatively insensible to the accuracy of the onboard model, yet it is vulnerable to the choice of the initial parameters. Slight changes in the parameters or a different flight scenario may largely affect the drag reduction capabilities of the PR-mode.

The second drag minimization mode (model-based, MB) incorporates the drag function in the control allocation problem and uses the excess control power to force the effectors to their minimum drag position. If the onboard model is precise the performance is comparable to that of the PR-mode, as it reduces drag with about 6.5%. With an inaccurate onboard model however the drag reduction is significantly less. In return the number of initial parameters is much less and the performance is rather insensitive to these parameters.

In conclusion, effector prioritization can be an effective way to reduce operational drag of an aircraft, but its efficiency depends on initial tuning. For practical application the technique is questionable because acceptable performance cannot be guaranteed over the entire flight envelope, especially not with one fixed set of parameters. On the other hand model-based drag reduction in control allocation design is theoretically substantiated and expected to maintain its performance in a much wider range of circumstances. The prerequisite is that the onboard model accurately estimates the actual behavior of the aircraft.

The tests in this study involved turning and aiming commands at subsonic speeds. A topic for future research is to investigate the performance of the modes in other parts of the flight envelope (e.g. supersonic speeds) and with other maneuvers. The most important recommendation is to improve the ICE aerodynamic model, such that physically implausible phenomena are corrected. A high fidelity model can expose the real potential of spline-based modeling and the opportunities for spline-based mission-specific control allocation for next generation fighter aircraft.

References

1. Dorsett, K. M. and Mehl, D. R., "Innovative control effectors (ICE), ADB212813," Tech. rep., Wright Laboratory, 1996.
2. Dorsett, K. M., Fears, S. P., and Houlden, H. P., "Innovative control effectors (ICE) phase II, ADB212813," Tech. rep., Wright Laboratory, 1999.
3. Durham, W. C., "Constrained control allocation," *Journal of Guidance, Control, and Dynamics*, Vol. 16, No. 4, 1993, pp. 717–725.
4. Buffington, J. M. and Enns, D. F., "Lyapunov stability analysis of daisy chain control allocation," *Journal of Guidance Control and Dynamics*, Vol. 19, No. 6, 1996, pp. 1226–1230.
5. Virnig, J. and Bodden, D., "Multivariable control allocation and control law conditioning when control effectors limit," *Guidance, Navigation, and Control Conference*, 1994, p. 3609.
6. Johansen, T. A. and Fossen, T. I., "Control allocation, a survey," *Automatica*, Vol. 49, No. 5, 2013, pp. 1087–1103.
7. Matamoros, I. and de Visser, C., "Incremental Nonlinear Control Allocation for a Tailless Aircraft with Innovative Control Effectors," *AIAA Guidance, Navigation, and Control Conference and Exhibit*, 2018, p. 1116.
8. Sieberling S, Chu, Q. and Mulder, J., "Robust Flight Control Using Incremental Nonlinear Dynamic Inversion and Angular Acceleration Prediction," *Journal of Guidance, Control, and Dynamics*, Vol. 33, No. 6, 2010, pp. 1732–1742.
9. Härkegård, O., "Efficient active set algorithms for solving constrained least squares problems in aircraft control allocation," *Proceedings of the 41st IEEE Conference on Decision and Control*, Vol. 2, IEEE, 2002, pp. 1295–1300.
10. Niestroy, M. A., Dorsett, K. M., and Markstein, K., "A Tailless Fighter Aircraft Model for Control-Related Research and Development," *AIAA Modeling and Simulation Technologies Conference*, 2017.
11. Tol, H., De Visser, C., Van Kampen, E., and Chu, Q., "Nonlinear multivariate spline-based control allocation for high-performance aircraft," *Journal of Guidance, Control, and Dynamics*, Vol. 37, No. 6, 2014, pp. 1840–1862.
12. van der Peijl, I. V., *Physical Splines for Aerodynamic Modelling of Innovative Control Effectors*, Master's thesis, Delft University of Technology, 2017.
13. Härkegård, O., *Backstepping and control allocation with applications to flight control*, Ph.D. thesis, Linköpings Universitet, 2003.
14. Prasad, K. M. and Bapat, R., "The generalized Moore-Penrose inverse," *Linear Algebra and its Applications*, Vol. 165, 1992, pp. 59–69.
15. Buffington, J. F., "Modular control law design for the innovative control effectors (ICE) tailless fighter aircraft configuration 101-3," Tech. rep., DTIC Document, 1999.